Accepted Manuscript

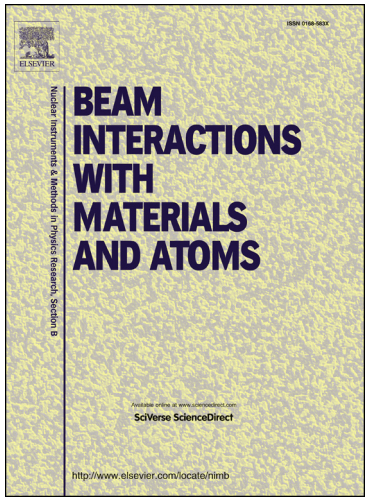

Barkas effect in the stopping power for ions with different ionization degrees

Claudio D. Archubi, Isabel Abril, Rafael Garcia-Molina, Néstor R. Arista

PII: S0168-583X(13)00904-X
DOI: http://dx.doi.org/10.1016/j.nimb.2013.08.034
Reference: NIMB 59825

To appear in: *Nucl. Instr. and Meth. in Phys. Res. B*

Please cite this article as: C.D. Archubi, I. Abril, R. Garcia-Molina, N.R. Arista, Barkas effect in the stopping power for ions with different ionization degrees, *Nucl. Instr. and Meth. in Phys. Res. B* (2013), doi: http://dx.doi.org/10.1016/j.nimb.2013.08.034

Barkas effect in the stopping power for ions with different ionization degrees

Claudio D. Archubi[1], Isabel Abril[2], Rafael Garcia-Molina[3], and Néstor R. Arista[4]

[1] *Instituto de Astronomía y Física del Espacio, C1428EGA, Buenos Aires, Argentina*

[2] *Departament de Física Aplicada, Universitat d'Alacant, Alacant E-03080, Spain*

[3] *Departamento de Física – Centro de Investigación en Óptica y Nanofísica, Universidad de Murcia, Murcia E-30100, Spain and*

[4] *Centro Atómico Bariloche and Instituto Balseiro, Comisión Nacional de Energía Atómica, 8400 Bariloche, Argentina*

(Dated: August 16, 2013)

Abstract

The Barkas effect in the electronic stopping power for dressed projectiles moving in a free electron gas is studied for a wide range of velocities v. The interaction of the projectile with the target is described using screened interaction potentials, which take into account the self screening due to the projectile bound electrons and the external screening produced by the target electron gas. The projectile trajectories are calculated using a classical simulation method, and the Barkas factor is obtained from the scattering of the target electrons in the potential of the projectile and that of its antiparticle, following the transport cross section model. A large set of numerical simulations were made for different projectiles, degrees of ionization and velocities. We find that the Barkas factor increases at high energies with the number of projectile bound electrons, whereas its velocity dependence changes from the v^{-3} behavior for bare projectiles to a v^{-2} behavior for neutral ones. Interesting effects of curve crossings in the Barkas factor at different degrees of ionization as a function of the projectile velocity are observed. A simple scaling law for neutral and fully ionized projectiles is also derived.

I. INTRODUCTION

During the last decades many theoretical studies have been published to explain the deviation of the electronic stopping power from the quadratic dependence on projectile charge Z_1 predicted by the Bethe theory [1] in the context of the plane wave Born approximation for bare ions. This deviation, called Barkas effect, was first experimentally observed in 1956 by Barkas and co-workers, who found a difference in the penetration ranges of positive and negative pions in matter [2]. After Barkas measurements, several other experimental studies have confirmed these deviations. Andersen *et al.* [3] explained differences between the stopping cross-sections measured for MeV alpha particles, protons and deuterons in Al, Cu, Ag and Au targets, considering a Z_1^3 contribution to the energy loss. More than a decade later, experiments by the Aarhus-CERN collaboration [4, 5] revealed very large differences between the stopping of protons and anti-protons in a silicon target. Detailed comparisons between theoretical predictions and experimental results have been reported by Bichsel [6, 7], who provided a set of quantitative analyses taking into account the influence of other relevant contributions to the stopping power, such as inner-shell and Bloch corrections, which may mask or distort the analysis of the pure Barkas effect. Further experiments by the group of Porto Alegre [8, 9] have provided valuable data on the Barkas effect for heavier ions (He, Li, Be and B) in channeling conditions.

From the theoretical point of view, one of the first descriptions of the Barkas effect was made by Ashley, Ritchie and Brandt [10], who extended to second-order terms the analysis of the electronic stopping power in a classical treatment similar to the Bohr model [11]. They argued that only distant collisions were relevant for contributions to higher order in Z_1, because in close collisions the electrons behave as if they were essentially free and their contribution to the Z_1^3 effect becomes small since the Rutherford cross section for free electrons is exactly proportional to Z_1^2.

Later on, Lindhard [12] showed that the effect of close collisions was about as important as the part corresponding to distant collisions. He considered a particle moving in a free electron gas and showed that an additional Z_1^3 term appears as a consequence of the screening of the electron gas around the projectile, which affects the dynamics of the scattering process.

After Lindhard's estimation [12], the contribution of close collisions to the Barkas effect was calculated by different approaches: using second-order quantum scattering theory [13],

by a non-linear response theory for quantum oscillators [14], using binary theory with a screening potential [15], by many-body theory [16], and by a classical scattering treatment for heavy ions interacting with a free electron gas [17].

In a more general picture, the analysis extended to Z_1^3 order has some limitations since the Bloch expression for the stopping power [12] produces an additional Z_1^4 term that in most cases becomes comparable in magnitude to the Z_1^3 term. It is also well known that, for heavy projectiles, the analysis based only on the Z_1^3 Barkas term is not enough to calculate all the non-linear effects in the stopping power, and a more complete expansion in powers of Z_1 is needed for this purpose. Other methods, such as the quantum scattering calculations based on the extended Friedel sum rule [18–20], the classical dynamics treatment [17], the binary theory model [15], the continuum-distorted-wave method [21–23], and the semiclassical WKB approximation [24] have also been employed to evaluate all the non-linear contributions to the stopping for heavy projectiles.

Most of these analyses were made assuming bare projectiles. As it is well known, the degree of ionization of a projectile moving in a target depends on its velocity. So at low and intermediate velocities the effect of the projectile bound electrons in the stopping power must be considered. In a phenomenological description, the stopping power may be assumed to be proportional to the square of an effective charge (in fact, the *effective charge* is empirically defined in this way). However the treatment based on the effective charge may be quite misleading [25]. A more systematic analysis of the effective-charge problem has been performed by Brandt and Kitagawa (BK) [26] using a dielectric response approximation. Their formulation uses a variational method considering a statistical model for the projectile in which the charge density is represented by a simple analytical expression. Other approximations for the interaction potential of moving ions have been used in various computer codes, such as the CASP, HISTOP and PASS. A recent survey and references on these codes can be found in Ref.[27]. In the present study we describe the electronic structure of the projectile by means of two different approaches: (i) for heavy ions we employ the BK model, because it allows the analytical treatment, in a statistical manner, of the electronic charge density for ions with many bound electrons, and (ii) for light ions, with few bound electrons, we use the model developed by Kaneko [28], which provides useful analytical expressions for the projectile electronic density taking into account the electronic shell structure by means of modified hydrogenic orbitals.

The purpose of this paper is to perform a detailed analysis of the Barkas effect in the stopping power for ions with different ionization degrees, at intermediate and high velocities, traversing a free electron gas corresponding to a metallic Al target. The study is based on a classical dynamics treatment and the transport cross section approach [17]. The present energy loss model has also some features in common with binary theory from Ref.[15]. The main difference is that our model is based on the hypothesis of collisions with a free electron gas, while the binary theory of Ref.[15] calculates collisions with bound electrons assuming a uniformly moving ion interacting with classical harmonic oscillators.

The interaction between the ionized projectiles and the target electrons is studied by numerical simulations of the electron trajectories, where the projectile is described using two different models [26, 28] and the target is modeled by a free electron gas. The approach is fully non-perturbative, so that a whole development in powers of Z_1 is implicitly included. Since the purpose of this work is to analyse the effects of the projectile's ionization degree on the Barkas effect, we will not consider hydrogen projectiles in our study. Low velocities are also excluded from our work, because our methodology is only applicable to velocities larger than the Fermi velocity of the target.

The paper is organized as follows. In Sect. II the theoretical approach of the transport cross section is described and the simulation procedure is explained. In Sect. III our calculations of the Barkas factor are presented for projectiles with different degree of ionization and velocities moving in an electron gas, represented by an aluminum target; a comparison with previous bare-ion descriptions is made. Finally, in Sect. IV the main conclusions of this work are summarized.

II. TRANSPORT CROSS SECTION AND SIMULATION METHOD

We consider an ion with velocity v and nuclear charge $Z_1 e$, carrying N bound electrons, moving through a free electron gas with a plasmon frequency $\omega_{\rm p}$. To describe the charge density of the ions two different approaches are used: (i) the statistical Brandt-Kitagawa model [26] for heavy ions, and (ii) the individual few-electron model from Kaneko [28] for light ions.

The charge density of the projectile $\rho_{tot}(r,t)$, screened by the medium, is given by

$$\rho_{tot}(r,t) = \rho_q(r - vt) + \rho_e(r - vt), \tag{1}$$

where ρ_q represents the charge density of the projectile with charge $q = (Z_1 - N)e$ screened by the electron gas whereas the second term ρ_e accounts for the N bound electrons of the projectile.

According to the BK model, ρ_e can be expressed as:

$$\rho_e(r) = -\frac{Ne}{4\pi\Lambda^3}\frac{\Lambda}{r}\exp\left(-r/\Lambda\right) \tag{2}$$

where Λ is the screening length of the bound electrons, given by [26]

$$\Lambda = \frac{0.48(N/Z_1)^{2/3}a_0}{Z_1^{1/3}\left[1 - \frac{1}{7}\left(N/Z_1\right)\right]}, \tag{3}$$

where a_0 is the Bohr atomic radius.

Considering that the ion charge $q = (Z_1 - N)e$ is screened by the electron gas, the following expression for $\rho_q(r)$ can be proposed:

$$\rho_q(r) = -\frac{(Z_1 - N)e\alpha^2}{4\pi r}\exp(-\alpha r). \tag{4}$$

Then, the differential equation for the interaction potential $V(r)$, given by

$$\nabla^2 V(r) = 4\pi e\rho_{tot}(r), \tag{5}$$

is solved, obtaining a sum of two Yukawa potentials

$$V(r) = -\frac{(Z_1 - N)e^2}{r}\exp(-\alpha r) - \frac{Ne^2}{r}\exp(-\gamma r). \tag{6}$$

The first term corresponds to the potential of the ion charge $q = (Z_1 - N)e$, screened by the target electrons, with a screening length $\lambda = 1/\alpha$, where $\alpha = \pi\omega_{\rm p}/2v$ [12], which depends on the projectile velocity v, and where $\omega_{\rm p}$ is the plasmon frequency of the target. The second term in equation (6) takes into account the internal screening due to the bound electrons of the projectile, where the screening length $\Lambda = 1/\gamma$ is given by Eq.(3). Notice that in this description both terms of the interaction potential are spherically symmetric. For a bare projectile the expression (6) reduces to the conventional Yukawa potential with a screening

length $\lambda = 2v/\pi\omega_{\rm p}$; on the other hand, if the projectile is a neutral atom the potential also reduces to a Yukawa term but with a different (smaller) screening length, Λ.

For light projectiles such as He or Li, where the use of the BK model is not appropriate due to its statistical assumptions, we have used individual ionic potentials for each projectile charge state, which were built from hydrogenic-like wavefunctions following the approach developed by Kaneko [28].

The trajectories of the electrons relative to the moving ion were calculated by means of a simulation method, where for practical purposes, we invert the problem and consider the scattering of electrons on a fixed screened ion, placing its center of mass at the position of the nucleus. Since we assume that the electrons were initially at rest in the target system (note that the present study is restricted to projectile velocities larger than the Fermi velocity of the metal target) and the projectile was moving with a velocity v, in the new frame of reference the electrons will start moving with an initial velocity $-v$.

Then, Newton's equation is numerically integrated following the algorithm of Euler-Cauchy [29] with a force given by the negative value of the gradient of the potential $V(r)$. In this manner, the trajectories of the incident electrons are calculated at different impact parameters b. Taking into account that the electron velocity changes appreciably during the collision and its trajectory becomes very sensitive to small changes in its position and velocity when it passes close to the (now static) projectile, a variable time step is used in the simulation which depends on the electron instantaneous velocity and on the distance to the projectile nucleus. The simulation of the electron trajectories allows to obtain the scattering angles $\theta(b, v)$, through the expression $\theta(b, v) = \arccos(u_x/u_f)$, where u_f is the electron final velocity in the scattering plane and u_x is its component along the initial direction of v.

Next, following the transport cross section method (TCS) of Ref.[17], we calculate the transport cross section,

$$\sigma_{\rm tr} = \int [1 - \cos\theta(b, v)]\, 2\pi b\, db. \tag{7}$$

Despite the fact that the contribution to the above integral from large values of the impact parameter b becomes almost negligible, to solve it numerically with accuracy, we extend the range of our simulations to values of b much larger than 10 a.u. for He and Li projectiles, and to 30 a.u. for Ne and Ar by means of an exponential extrapolation.

In order to determine the Barkas effect, which measures the asymmetry in the stopping

of particles and their corresponding antiparticles, the scattering problem for the image ion potential is solved with the same numerical procedure, where the new potential is obtained by simply changing the sign of the total potential of the ion. Finally, using the relation between the mean energy loss per unit path length $S = -\mathrm{d}E/\mathrm{d}x$ and the transport cross section for swift ions, $S = nm_e v^2 \sigma_{\mathrm{tr}}$ [30] (where n is the electron density of the target and m_e is the electron mass), we obtain the Barkas factor from the simulations of the scattering of target electrons in the potential of the projectile (Z_1) and its image ($-Z_1$), namely

$$R_{\mathrm{Barkas}} = \frac{\sigma_{\mathrm{tr}}(Z_1) - \sigma_{\mathrm{tr}}(-Z_1)}{\sigma_{\mathrm{tr}}(Z_1) + \sigma_{\mathrm{tr}}(-Z_1)}, \tag{8}$$

where σ_{tr} is calculated according to Eq.(7). Note that the Barkas factor depends also on the degree of ionization $q = (Z_1 - N)e$ of the projectile, which affects the interaction potential, Eq.(6), and therefore the scattering angle $\theta(b, v)$. Therefore, in this work the Barkas effect is quantified by the Barkas factor.

III. RESULTS

Using the previously described method, we have performed a large set of simulations for many impact parameters b, assuming different projectiles velocities v, atomic numbers Z_1, and number of bound electrons N, in a free electron gas target with the plasma frequency of aluminum (ω_{p}=0.551 a.u. = 14.99 eV), which is representative of a free electron gas.

First of all we check the values of the projectile interaction potentials obtained from individual ionic potentials from Kaneko's model [28] or from the Brandt-Kitagawa model [26] for light projectiles such as He and Li. We show in Fig. 1 the interaction potential $V(r)$ versus the distance r for (a) $\mathrm{He}^{0,1+}$ and (b) $\mathrm{Li}^{0,1+,2+}$, impinging with velocity $v = 2$ a.u. on an Al target. Even though the statistical Brandt-Kitagawa model is suitable only for heavy projectiles, we find a remarkable similarity between the BK values (lines) and the individual ionic potentials (symbols) also in the case of light ions such as He^{1+}, Li^{1+} and Li^{2+}. However for neutral projectiles (He^0 and Li^0) the discrepancies between both potential models are larger and increase with the distance. This may be attributed to a failure of the statistical BK model for these cases. The dependence of the interaction potential with the velocity of the projectile is also analyzed in Fig. 1, where panel (c) corresponds to He^+ and (d) to Li^{2+} with velocities $v = 2$ a.u. and 6 a.u. We note in these latter panels that

the interaction potential increases with the projectile velocity (which corresponds actually to weaker screening conditions) due to the larger values of the dynamical screening length $\lambda = 2v/\pi\omega_{\rm p}$.

In Fig. 2 we show the integrand of the transport cross section, Eq.(7), $f(b) = 2\pi b[1 - \cos\theta(b, v)]$ as a function of the impact parameter b for He projectiles with velocity $v = 2$ a.u. moving in an Al free electron gas. We compare, in panels (a) to (c), the function $f(b)$ for different degrees of ionization of the He projectiles as well as its corresponding anti-particles $\overline{\rm He}$. These calculations show that a large contribution to the transport cross section comes from small impact parameters, which explain why the charge state effects are important in $\sigma_{\rm tr}$. Also, it is interesting to notice that when the projectile loses its bound electrons (panel c) the range of impact parameters that contribute to $\sigma_{\rm tr}$ increases, as a consequence of the larger spread in the screening produced by the free electrons (as compared with that of bound electrons). It is also clear from this comparison that the case of neutral projectiles (panel a) shows a more compact spatial distribution and a larger difference in the areas under the solid and the dashed curves (i.e., a larger Barkas effect).

The calculated Barkas factor $R_{\rm Barkas}$, obtained from Eq.(8), is shown in Fig. 3 as a function of the projectile velocity for several projectiles (He, Li, Ne and Ar) with different degrees of ionization moving in an aluminum target. The main feature is that the value of Barkas factor increases with the number of bound electrons at intermediate or high velocities, depending on the ion. The physical reason of this effect is that the screening of bound electrons occurs at shorter distances and hence the deviations from the Rutherford scattering are stronger. This behavior is in agreement with results obtained using a semiclassical approach [24].

Additionally, we note that for a given projectile, there is a crossing at low or intermediate velocities between the Barkas factor curves corresponding to different degrees of ionization. This feature is clear in Fig. 3 for heavy projectiles such as Ne and Ar, and it also occurs for light projectiles at lower energies (not shown in the figure). Note that we restrict our analysis here to intermediate and high energies since the present approach fails at low energies. The reason of this behavior is that the screening length $\lambda = 2v/\pi\omega_{\rm p}$ in the first term of the interaction potential (see Eq.(6)) decreases at low velocities, producing a competition between the two Yukawa terms of the interaction potential.

Hence, whereas at high velocities the first term of the potential dominates the Barkas

effect (since γ is constant while λ increases), at lower velocities λ decreases significantly and the second Yukawa term becomes also important. This fact explains why the Barkas factor curves show different behavior depending on the degree of ionization of the projectile and a crossing between different curves may eventually appear. We have additionally confirmed the occurrence of such curve crossings using analytical expressions for the Barkas factor derived from simpler potentials such as the Mensing potential [17] and considering different screening lengths.

Also, we note that the Barkas factor increases with the atomic number of the projectile as shown in Fig.3 (see the different scales in the panels). For light projectiles (He and Li), we have also included in Fig. 3 the Barkas factor obtained from individual ionic potentials from Kaneko's model (dashed lines) and from the Brandt-Kitagawa model (solid lines). Another remarkable difference observed in Fig. 3 is the change in the slope of the various curves at high energies. In particular, we find a dependence of the Barkas factor of the type $\propto v^{-2}$ for neutral projectiles, quite different from the $\propto v^{-3}$ behavior characteristic of bare ions [12].

For bare ions, the basic parameter in the Lindhard formulation [12] is the scaling parameter $\varsigma = \pi Z_1 e^2 \omega_{\rm p}/m_e v^3$ which is obtained as the ratio between the collision radius ($Z_1 e^2/m_e v^2$) and the screening length ($\lambda = 1/\alpha$). In the case of neutral projectiles ($N = Z_1$), the interaction potential given by Eq.(6) also reduces to a standard Yukawa potential, hence the scaling parameter should be replaced (following the arguments proposed by Lindhard [12]) by $\varsigma' = 2N\gamma/m_e v^2$, as explained in the Appendix. Notice that both scaling parameters are dimensionless but they have different characteristics; for bare projectiles, the dependence of ς on Z_1 is linear, while for neutral projectiles the scaling parameter ς' is not linear on the number of bound electrons N, since the screening parameter $\gamma = 1/\Lambda$, given by Eq.(3), also depends on N. The dependence of the scaling parameter with the projectile velocity is also different for bare or neutral projectiles: for bare ions $\varsigma \propto v^{-3}$ whereas for neutrals $\varsigma' \propto v^{-2}$.

To illustrate the scaling property, the Barkas factor $R_{\rm Barkas}$ is shown in Fig. 4 as a function of the scaling parameter $Z_1/\beta v^2$ for bare projectiles He^{2+}, Li^{3+}, Ne^{10+}, and for neutrals He^0, Li^0, Ne^0, where $\beta = 1/2\alpha$ for bare projectiles and $\beta = 1/2\gamma$ for neutral ones. We obtain a close coincidence of the simulated Barkas factor for all the projectiles, in agreement with the scaling prediction. However, at intermediate degrees of ionization ($0 < N < Z_1$) no such simple scaling law was found. Notice that for all projectiles there is a *saturation effect* in the Barkas factor for $Z_1/\beta v^2 \sim 5$, so that an additional increase in the value of Z_1 produces

a decrease of the Barkas effect. This effect, not predicted by the usual Z_1^3 term analysis, has also been observed in previous calculations and measurements [8, 9, 20] and is due to the contribution of higher order terms of the expansion in powers of Z_1. Since the present method includes all order terms in the interaction strength, the saturation effect is clearly observed. Finally, we note that in particular this analysis also explains the change from the $\propto v^{-3}$ to the $\propto v^{-2}$ behavior at high energies (for bare and neutral projectiles) discussed in the previous paragraph.

In a more realistic analysis, the effective number of bound electrons N depends on the nature and velocity of the projectile and on the target. Experimentally the mean ion charge q in all materials increases with the projectile velocity, and at high velocities tends to the atomic number Z_1. Therefore, we define the velocity dependent average Barkas factor $\langle R_{\rm Barkas}\rangle$ as

$$\langle R_{\rm Barkas}\rangle(v) = \sum_{q=0}^{Z_1} \phi_q(v) R_{\rm Barkas}(q,v), \tag{9}$$

where $R_{\rm Barkas}(q,v)$ represents the value of the Barkas factor (see Eq.(8)) for a projectile with a degree of ionization q and velocity v, and $\phi_q(v)$ are the charge-state fractions of the projectile, which depend on the target, the projectile and its velocity. Here we used the equilibrium charge-state fractions obtained by a parameterization of experimental data [31]. The results corresponding to the average Barkas factor is presented in Fig. 5 by solid lines for He, Li, Ne and Ar projectiles moving in an aluminum target, as a function of the projectile energy. For comparison purposes, results corresponding to bare projectiles are also been depicted by dotted lines. We observe that $\langle R_{\rm Barkas}\rangle$ diminishes with the projectile energy for intermediate and high energies. This behavior has two reasons: the first is the "normal behavior" predicted by the Lindhard analysis for bare projectiles, which predicts the approach to the Rutherford (Z_1^2) limit at high energies; the second reason is that as the energy increases the effective number of bound electrons decreases, and, as it was shown before, the weakening of the screening by bound electrons also produces a decrease of the Barkas effect. At high energies, the results for $\langle R_{\rm Barkas}\rangle$ approach those for bare ions.

Finally, we note that for heavier projectiles such as Ne and Ar, the average Barkas factor $\langle R_{\rm Barkas}\rangle$ shows a crossing with the curves corresponding to bare projectiles at intermediate energies. These crossings are a consequence of the behavior observed in Fig. 3 for these

projectiles, since the values of $\langle R_{\rm Barkas} \rangle$ were calculated using the corresponding percentages of the results for ionized projectiles shown in that figure. Hence, the reason for these crossings is also a consequence of the competition between the two terms with different screening lengths in the potential of Eq.(6). This shows that the normal behavior observed at high energies may be reversed for heavy projectiles at lower energies.

IV. CONCLUSIONS

We have performed a large series of classical simulations of electron scattering by ions moving through a free electron gas considering various cases of light and heavy ions with different charge states and for a wide range of velocities. From these numerical simulations we have obtained a set of new results that provide useful information on the form of the Barkas factor at intermediate and high velocities.

As a general conclusion, the analysis of our results shows that at large projectile velocities, the Barkas factor increases with the number of bound electrons (for the same element), in agreement with previous results obtained with a semiclassical treatment [24]. We show that this effect is due to the more effective screening produced by bound electrons.

The velocity dependence of the Barkas factor at high velocities shows a significant change, decreasing as v^{-3} in the case of bare ions and as v^{-2} in the case of neutral projectiles.

In addition, we find a change of behavior of the Barkas factor for heavy ions at intermediate velocities, where a crossing of curves corresponding to different ionization degrees is obtained. This effect is due to changes in the screening conditions represented by two different screening length, one of short range which accounts for the projectile core, and another of long range corresponding to the collective screening by the target electrons, which depends on the projectile velocity.

Finally, the scaling analysis performed here (see Appendix) reveals a unified behavior of bare and neutral projectiles when the Barkas factors are represented in terms of the appropriate scaling parameters.

Because of the simplifying free-electron-gas assumption we did not include here comparisons with experimental results, which may be the subject of a much more extended study.

V. APPENDIX: LINDHARD'S SCALING ARGUMENT

The interaction potential for bare projectiles with atomic number Z_1 and velocity v, moving through a free electron gas with plasma frequency $\omega_{\rm p}$, can be approximated by the well known Yukawa potential for a screened point charge, that is

$$V_{\rm bare}(r) = -\frac{Z_1 e^2}{r}\exp(-\alpha r), \tag{10}$$

where $\alpha = \pi\omega_{\rm p}/2v$. Applying Lindhard's argument [12], an expansion for $r \to 0$ is made, giving

$$V_{\rm bare}(r) \cong -\frac{Z_1 e^2}{r}(1-\alpha r) = -\frac{Z_1 e^2}{r} + V_1, \tag{11}$$

where $V_1 = Z_1 e^2 \alpha$. This correspond to the following shift in the electron kinetic energy

$$\frac{1}{2}m_e v^{*2} = \frac{1}{2}m_e v^2 - V_1 = \frac{1}{2}m_e v^2\left(1 - \frac{2V_1}{m_e v^2}\right) = \frac{1}{2}m_e v^2(1-\varsigma), \tag{12}$$

where $\varsigma = 2V_1/m_e v^2 = \pi Z_1 e^2 \omega_{\rm p}/m_e v^3$ is Lindhard's scaling factor.

On the other hand, for neutral projectiles the interaction potential $V(r)$, given by eq.(6), reduces to another Yukawa potential with the following form

$$V_{\rm neutral}(r) = -\frac{Ne^2}{r}\exp(-\gamma r), \tag{13}$$

where

$$\gamma = \frac{N^{1/3}}{0.48}\frac{6}{7}\frac{1}{a_0}, \tag{14}$$

where $a_0 = 0.529$ Å is the Bohr radius. The shift in the electron kinetic energy is now given by

$$\frac{1}{2}m_e v^{*2} = \frac{1}{2}m_e v^2 - V_2 = \frac{1}{2}m_e v^2(1-\varsigma'), \tag{15}$$

where $V_2 = Ne^2\gamma$ and with $\varsigma' = 2V_2/m_e v^2 = 2N\gamma/m_e v^2$ the new scaling factor for neutral projectiles.

---

[1] H. Bethe, Ann. Phys. (Leipzig) **5**, 325 (1930).

[2] W. H. Barkas, W. Birnbaum and F. M. Smith, Phys Rev. **101**, 778 (1956); W. H. Barkas, N. J. Dyer and H. H. Heckman, Phys. Rev. Lett. **11**, 26 (1963).

[3] H. H. Andersen, J. F. Bak, H. Knudsen and B. R. Nielsen, Phys.Rev. A **16**, 1929 (1977).

[4] S. P. Møller, Nucl. Instrum. Meth. B **48**, 1 (1990).

[5] S. P. Møller, E. Uggerhøj, H. Bluhme, H. Knudsen, U. Mikkelsen, K. Paludan and E. Morenzoni, Phys. Rev. A **56**, 2930 (1997); Nucl. Instrum. Meth. B **122**, 162 (1997).

[6] H. Bichsel, Phys. Rev. A **41**, 3642 (1990).

[7] H. Bichsel, Phys. Rev. A **46**, 5761 (1992).

[8] G. de M. Azevedo, P. L. Grande, M. Behar and G. Schiwietz, Phys. Rev. Letter 86, 1482 (2001)

[9] L. L. Araujo, P. L. Grande, M. Behar, J. F. Dias, A. F. Lifshitz, N. R. Arista and G. Schiwietz, Phys. Rev. A 70, 032903 (2004)

[10] J. C. Ashley, R. H. Ritchie and W. Brandt, Phys. Rev. B **5**, 2393 (1972).

[11] N. Bohr, Philos. Mag. **25**, 10 (1913).

[12] J. Lindhard, Nucl. Instrum. Meth. **132**, 1 (1976).

[13] N. R. Arista, Phys. Rev. A **26**, 209 (1982).

[14] H. H. Mikkelsen and P. Sigmund, Phys. Rev. A **40**, 101 (1989); H. Esbensen and P. Sigmund, Ann. Phys. (N.Y.) **201**, 152 (1990).

[15] P. Sigmund and A. Schinner, Nucl. Instrum. Meth. B **212**, 110 (2003); P. Sigmund, A. Sharma, A. Schinner and A Fettouhi, Nucl. Instrum. Meth. B **230**, 1 (2005).

[16] J. M. Pitarke, R. H. Ritchie and P. M. Echenique, Phys. Rev. B **52**, 13883 (1995).

[17] N. R. Arista, P. L. Grande and A. F. Lifschitz, Phys. Rev. A **70**, 042902 (2004).

[18] A. F. Lifschitz and N. R. Arista, Phys. Rev. A **57**, 200 (1998); Phys. Rev. A **58**, 2168 (1998).

[19] N. R. Arista and A. F. Lifschitz, Phys. Rev. A **59**, 2719 (1999).

[20] N. R. Arista, Nucl. Instrum. and Meth. B **195**, 91-105 (2002).

[21] D. G. Arbó, M. S. Gravielle and J. E. Miraglia, Phys. Rev. A **62**, 032901 (2000).

[22] D. G. Arbó, M. S. Gravielle and J. E. Miraglia, Phys. Rev. A **64**, 022902 (2001).

[23] J. E. Miraglia and M. S. Gravielle, Phys. Rev. A **72**, 042902 (2005).

[24] N. R. Arista and P. Sigmund, Phys. Rev A **76**, 062902 (2007).

[25] A. F. Lifschitz and N. R. Arista, Phys. Rev. A **69**, 012902 (2004).

[26] W. Brandt and M. Kitagawa, Phys. Rev. B **25**, 5631 (1982); W. Brandt, Nucl. Instrum. Meth.

194, 13 (1982).

[27] H. Paul, Theory of Heavy Ion Collision Physics in Hadron Therapy (Chapter 2), Advances in Quantum Chemistry, vol. 65, page 39 (2013), Edited by D. Belkic, Academic Press (N.Y., 2013).

[28] T. Kaneko, Phys. Rev. A **49**, 2681 (1994).

[29] W. Eckstein, *Computer Simulation of Ion-Solid Interactions*, Springer-Verlag, Berlin (1991).

[30] P. Sigmund, Phys. Rev. A **26**, 2497 (1982).

[31] G. Schiwietz and P. L. Grande, Nucl. Instrum. Meth. B **175-177**, 125 (2001).

FIG. 1: (Color online) Interaction potential $V(r)$ *versus* the distance r for (a) He^0 and He^+, (b) Li^0, Li^+ and Li^{2+} moving with $v = 2$ a.u. in an electron gas of aluminum. The symbols show $V(r)$ for individual ionic potentials for light ions from Kaneko's model [28] whereas the lines correspond to the Brandt-Kitagawa potential [26]. $V(r)$ is shown in panel (c) for He^+ and (d) Li^{2+} projectiles moving in aluminum with velocities $v = 2$ a.u. and 6 a.u.

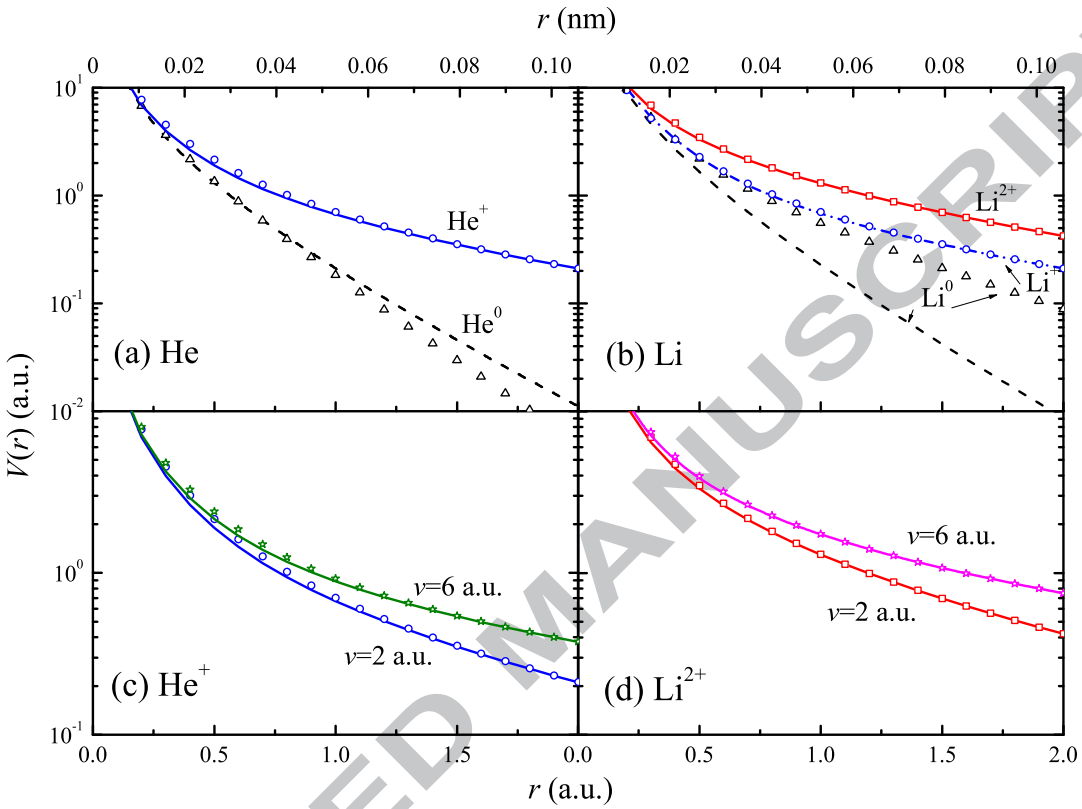

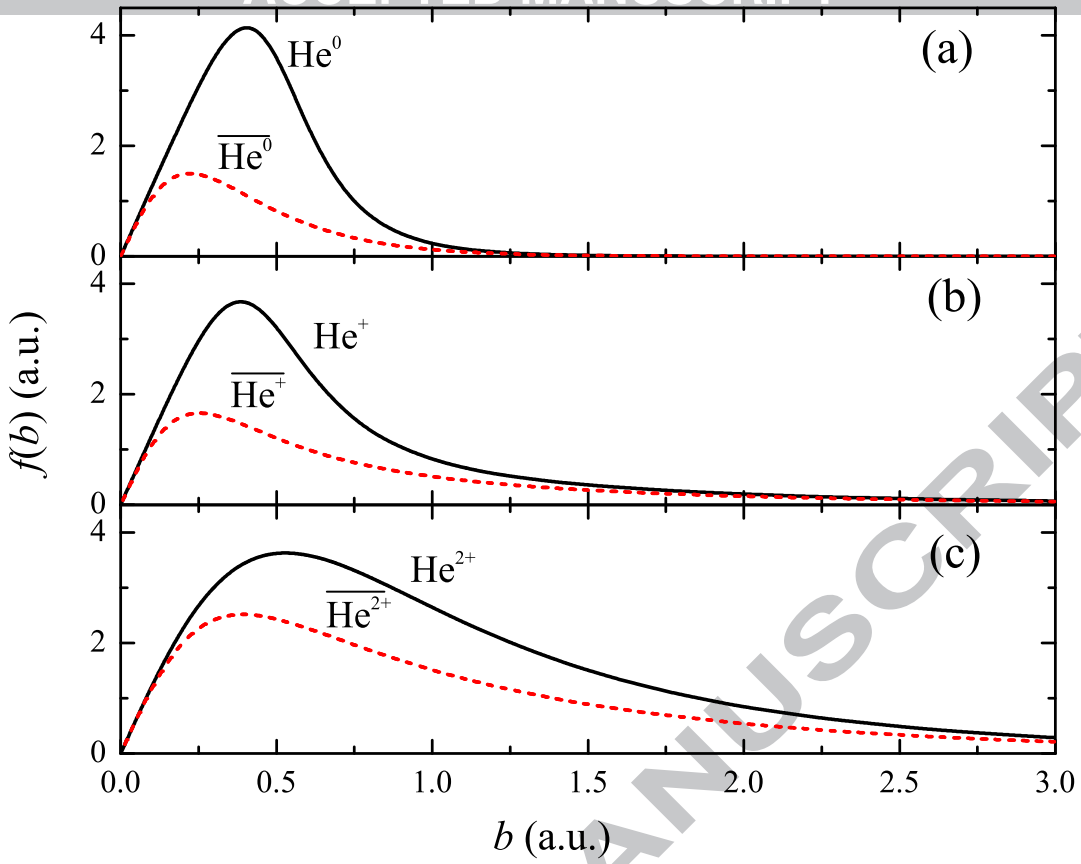

FIG. 2: (Color online) Function $f(b) = 2\pi b[1 - \cos\theta(b, v)]$ of Eq.(7) *versus* the impact parameter b for He projectiles with velocity $v = 2$ a.u. moving in an Al free electron gas for the three charge states of He. The curves of $f(b)$ for particles are shown by solid lines and those of the corresponding anti-particles by dashed lines.

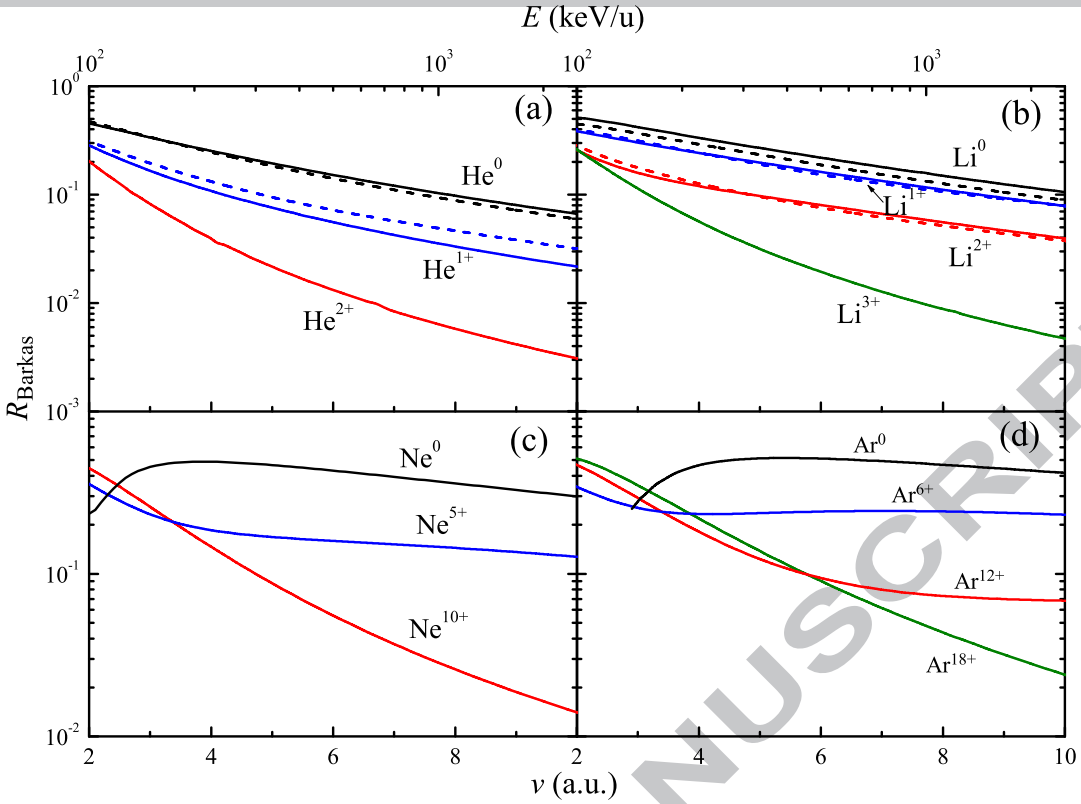

FIG. 3: (Color online) Velocity dependence of the Barkas factor R_{Barkas} for (a) He, (b) Li, (c) Ne and (d) Ar projectiles impinging on an electron gas of aluminum at different degrees of ionization. Solid lines represent the results for the Brandt-Kitagawa potential [26], whereas dashed lines correspond to individual ionic potentials for light ions from Kaneko's model [28].

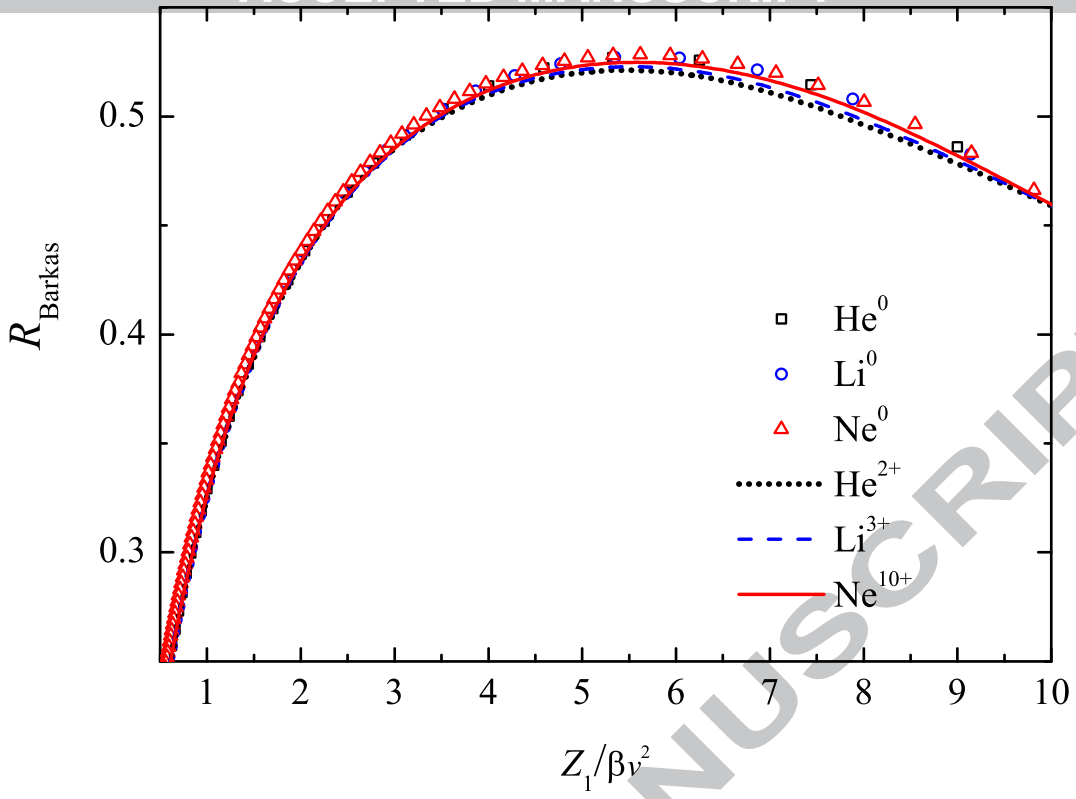

FIG. 4: (Color online) Calculations of the Barkas factor R_{Barkas} versus the screening parameter $Z_1/\beta v^2$ for He, Li, Ne bare projectiles (lines) and for neutral projectiles (symbols) impinging on an aluminum target. See the text for more details.

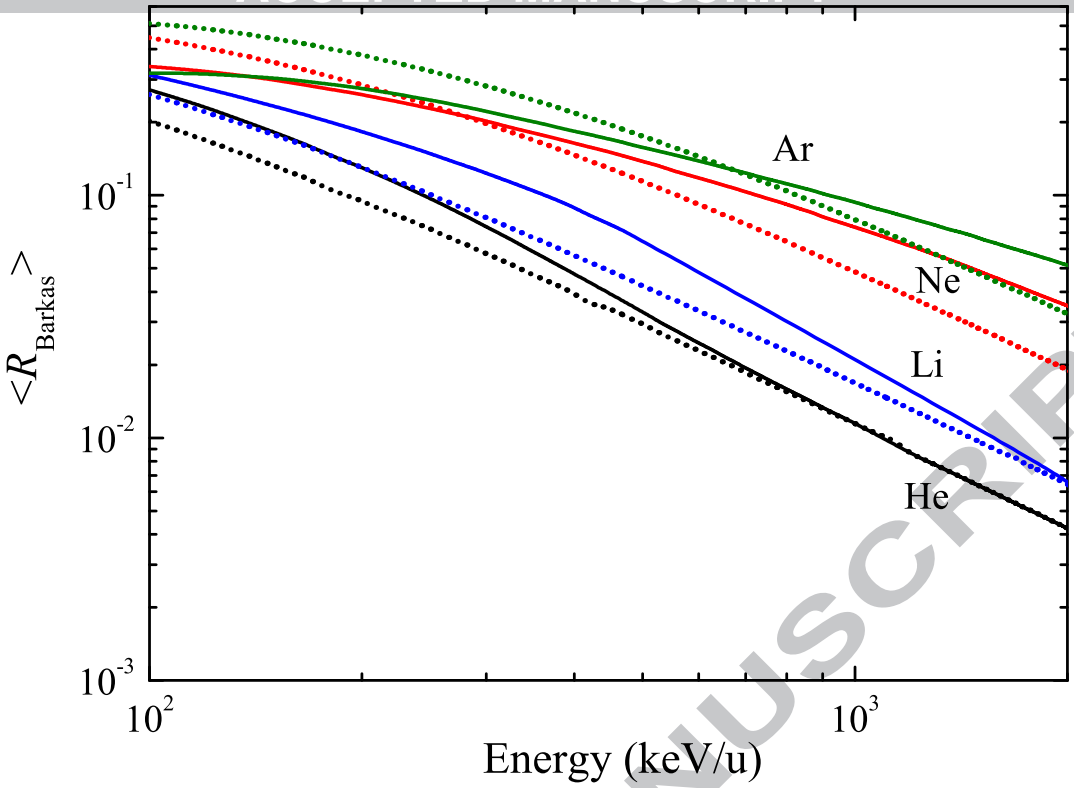

FIG. 5: (Color online) The average Barkas factor for He, Li, Ne and Ar projectiles impinging on an aluminum target as a function of energy is depicted by solid lines. For comparison purposes, dotted lines represent the Barkas factor for bare projectiles.